

Effect of Zn content on microstructure and mechanical performance in $\text{Bi}_{1.8}\text{Sr}_2\text{Ca}_2\text{Cu}_{3.2-x}\text{Zn}_x\text{O}_{10+\delta}$ glass ceramic

H. Koralay · O. Hicyilmaz · S. Cavdar ·
E. Asikuzun · A. T. Tasci · O. Ozturk

Received: 31 March 2014 / Accepted: 5 May 2014 / Published online: 17 May 2014
© Springer Science+Business Media New York 2014

Abstract In this study, we have investigated the effects of Zn doping on structural and mechanical properties of $\text{Bi}_{1.8}\text{Sr}_2\text{Ca}_2\text{Cu}_{3.2-x}\text{Zn}_x\text{O}_{10+\delta}$ ceramic samples with $x = 0.0, 0.1, 0.5, 1.0$. The prepared samples were characterized by using scanning electron microscope (SEM), energy dispersive spectroscopy (EDS), X-ray powder diffractometer (XRD) and static microhardness indenter. Surface morphology, orientation of grains and elemental composition analysis of the samples were investigated by SEM and EDS measurements, respectively. Texturing and lattice parameters a , b and c were determined from the XRD measurements. In this work we focused on Vickers microhardness measurements in order to characterize the mechanical properties. Experimental results of Vickers microhardness measurements were analyzed by using Meyer's law, the elastic/plastic deformation model, proportional sample resistance model (PSR), modified PSR model, Hays–Kendall (HK) approach and indentation induced cracking (IIC) model. According to the obtained results, HK approach is the most suitable model for the CZn00 sample showing indentation size effect behavior and IIC Model is the most suitable model for the CZn01, CZn05 and CZn10 samples showing reverse indentation size effect behavior.

1 Introduction

Since the discovery of superconductivity in the Bi–Sr–Ca–Cu–O (BSCCO) superconductor materials, they have been studied extensively in order to improve their superconducting optical and structural properties [1]. The properties as structural, physical and mechanical of BSCCO materials can be changed by substitution or addition of dopants having different ionic radii and different bonding properties [2]. The mechanical and other properties are either improved or destroyed depending on the characteristics of the dopant in the crystal structure. There have been several studies by substitution or addition of materials on the BSCCO system, but in general, it is mainly focused on 2223 system in the literature [3–5].

Microhardness is a mechanical property that gives useful information about the material composition as well as elastic modulus, yield strength and fracture toughness. The most convenient method of microhardness determination is the Vickers indentation method [6–12]. Vickers microhardness test is applied to different kind of materials (superconductors, ceramics, semiconductors, thin films, polymers and alloys) [6–9, 13].

It is well known that the microhardness of materials depends on the applied indentation test load, which is known as indentation size effect (ISE). ISE behavior occurs when the microhardness value of material decrease with the increase of applied test load [10–12, 14, 15]. In order to describe the ISE behavior of materials, several models including Meyer's law, proportional sample resistance (PSR), modified PSR (MPSR), elastic/plastic deformation (EPD) models and Hays–Kendall (HK) approach have been reported in the literature for the relation between the applied indentation test load F and indentation diagonal length d [16–18]. In contrast to ISE, another case is defined

H. Koralay (✉) · O. Hicyilmaz · S. Cavdar
Superconductivity and Thermal Analysis Laboratory,
Department of Physics, Faculty of Sciences, Gazi University,
06531 Ankara, Turkey
e-mail: hkoralay@gmail.com

E. Asikuzun · A. T. Tasci · O. Ozturk
Department of Physics, Faculty of Arts and Sciences, Kastamonu
University, 37100 Kastamonu, Turkey

as reverse indentation size effect (RISE), where the microhardness value increases with increasing the applied test load [19–22]. There are some models explaining this model in the literature, but the most successful one is indentation induced cracking (IIC) model.

In this study, we have investigated the effects of Zn doping on structural and mechanical properties of $\text{Bi}_{1.8}\text{Sr}_2\text{Ca}_2\text{Cu}_{3.2-x}\text{Zn}_x\text{O}_{10+\delta}$ glass ceramic samples with $x = 0.0, 0.1, 0.5, 1.0$. Microstructural properties of ceramic samples were investigated by X-ray diffraction (XRD), scanning electron microscopy (SEM) and energy dispersive spectrometer (EDS) measurements. Mechanical properties of the samples were characterized by Vickers microhardness test using the digital microhardness device by taking into account Meyer's law, PSR, MPSR, EPD, IIC models and HK approach.

2 Experimental procedures

First of all, $\text{Bi}_{1.8}\text{Sr}_2\text{Ca}_2\text{Cu}_{3.2-x}\text{Zn}_x\text{O}_{10+\delta}$ glass ceramic samples with $x = 0.0, 0.1, 0.5$ and 1.0 were produced. To obtain homogeneous mixture appropriate stoichiometric proportions of high purity Bi_2O_3 , PbO , SrCO_3 , CaCO_3 , CuO and ZnO powders were mixed in an agate mortar for 1 h. Then, put into an alumina crucible and heated up to $1,150\text{ }^\circ\text{C}$ with a step of $10\text{ }^\circ\text{C}/\text{min}$ heating rate from room temperature in a programmable furnace. The molten mixture was poured between two cooled copper plates to obtain about $0.6\text{--}0.8\text{ mm}$ of thick glasses after it was kept at $1,150\text{ }^\circ\text{C}$ for 1.5 h. Finally, the samples were sintered at $830\text{ }^\circ\text{C}$ for 120 h in a programmable tube furnace under an oxygen flow to obtain the ceramic samples crystal structure. Hereafter, for the samples with $x = 0.0, 0.1, 0.5$ and 1.0 , we will use the abbreviations CZn00, CZn01, CZn05 and CZn10, respectively.

Bruker D8 Advance X-ray powder diffractometer were used to characterize the lattice parameters of the samples with Cu-K_α radiation in the range of $3^\circ \leq 2\theta \leq 70^\circ$ at a scan speed of $2^\circ/\text{min}$. Surface morphology and grain orientations of the samples were determined by using Leo EVO-40 VPX scanning electron microscopy. In addition, the elemental composition analyses of the samples were analytically investigated by the energy dispersive spectrometer.

Vickers microhardness measurements were performed using the digital microhardness device at room temperature in order to determine the doping effect on the mechanical properties of the samples. The applied load, F , was changed within the range of $0.245\text{--}2.940\text{ N}$ and applied for 10 s. Indenter was suppressed on the different surfaces of the sample. The hardness models in the literature were analyzed using the calculated Vickers microhardness

values to determine the most appropriate model for the samples.

3 Results and discussion

3.1 XRD analysis

X-ray powder diffractometer graphs of the CZn00, CZn01, CZn05 and CZn10 samples are given in Fig. 1. Bi-2212 (041-0932-ICDD) main phase and SrO (074-1227 ICDD) impurity phase were determined for the undoped sample. With the increase in Zn addition, the peak intensity of the doped samples increases and other new peaks start to appear. Some of these peaks are Bi-2201 (046-0040ICDD), CuO (078-0428-ICDD) and CaSrO (048-1471 ICDD) impurity peaks and the others are unidentified impurity peaks.

The crystal structure was found to be orthorhombic for the samples. Calculated lattice parameters were given in Table 1. As can be seen from Table 1, lattice parameter a increases, however, b and c parameters initially increases and then decreases with Zn addition. This situation also was shown in Fig. 2. Lattice parameter a , in undoped sample, increases from 5.40 to 5.48 Å and c parameter initially increases from 30.78 to 30.83 Å, then decreases to 30.57 Å. Related to these parameters, lattice volume initially increases from 897.55 to 902.34 Å³ afterwards, decreases to 887.88 Å³ for CZn10 sample.

3.2 SEM analysis

The surface structure, grain sizes, accumulation in the grain boundaries and orientations of all samples were investigated by SEM images. As can be seen from Fig. 3, crystallization of the sample increases with the increase of Zn doping. Consequently, needle like and flaky like grains occurs. As seen from the figure, the granular morphology of the samples shows clear and needle like grains with layered growth. The composition of the needle like grains are believed to be due to the Bi-2223 phase. In all samples needle like grains are more dominant than flaky like grains. Needle like grains completely disappeared in CZn10 sample, which crystallized partially and the amorphous matrix began to degrade.

3.3 EDS analysis

Energy dispersive spectroscopy (EDS) is used to investigate the elemental composition analyses of the samples prepared in this work. The element concentration of the samples CZn00 ($x = 0.0$) and CZn10 ($x = 1.0$) are given in Fig. 4. In Table 2, variation of element concentrations

Fig. 1 XRD patterns of the samples

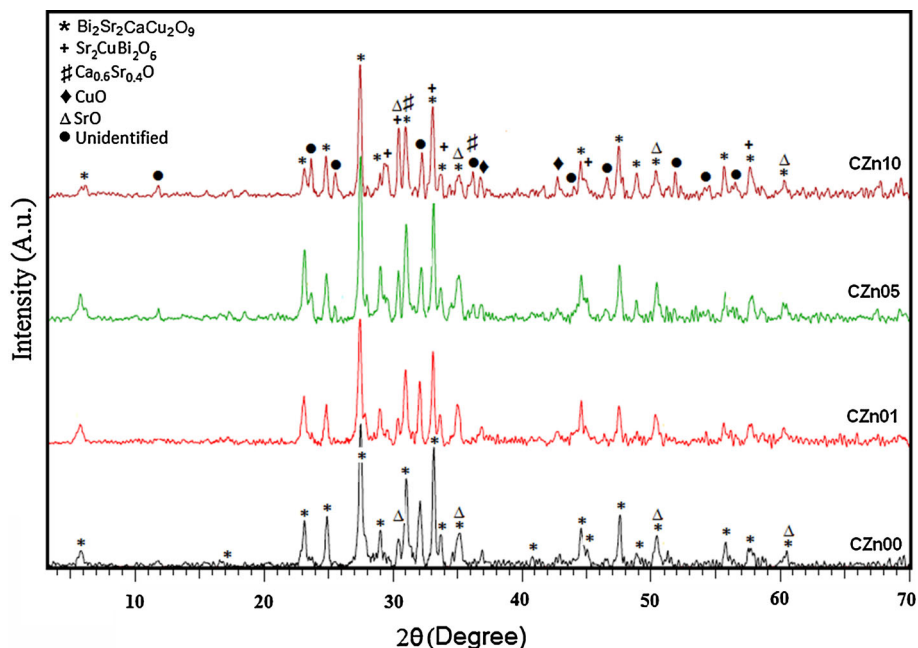


Table 1 Lattice parameters a , b , c and volume (V) values of all samples

Samples	V (\AA^3)	a (\AA)	b (\AA)	c (\AA)
CZn00	897.55	5.40	5.40	30.78
CZn01	899.50	5.41	5.40	30.79
CZn05	902.34	5.41	5.41	30.82
CZn10	887.88	5.48	5.30	30.57

from EDS measurements for CZn00 and CZn10 samples are given. As can be seen from Table 2, Zn concentration in sample $x = 1.0$ is increased with decreasing Cu and Ca concentration. However the reduction in Cu ions is more dominant. According to these results, the Zn atoms enter into the crystal structure by replacing Cu atoms [23, 24].

3.4 Vickers microindentation data analysis

The most general test on the materials is measurement of the hardness. Main reason for this, it is a simple test and destroys less than other test methods. Another advantage is that microhardness of the material has a parallel relationship with other mechanical properties. Hardness that is defined as the resistance of the materials against to abrasion, cut and puncture is a relative measure. The hardness value obtained using special devices in laboratories is resistance against to plastic deformation of the material. Brinell, Knopp and Vickers microhardness tests are commonly used hardness measurement methods applied in laboratories.

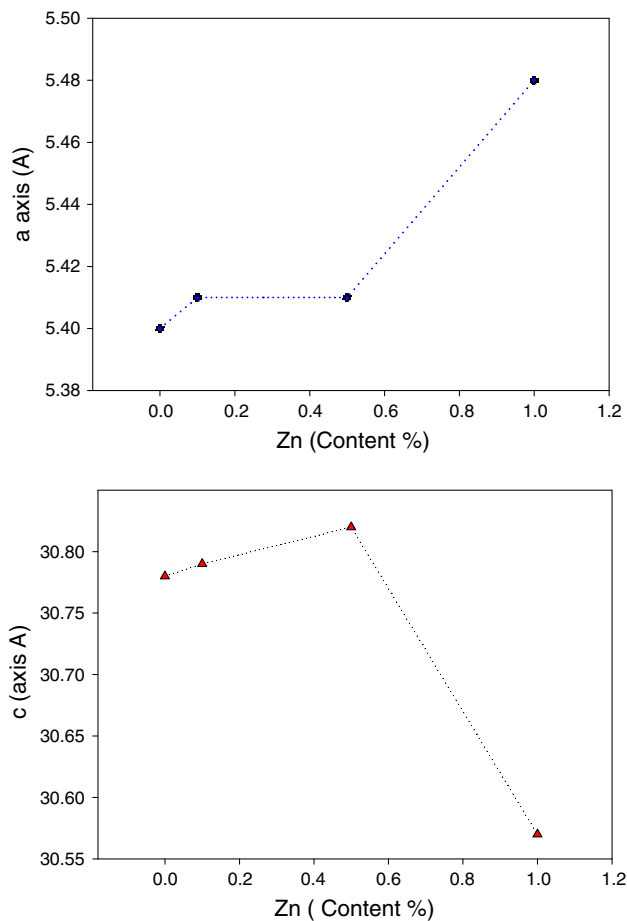


Fig. 2 Variation of the a and c lattice parameters with Zn doping

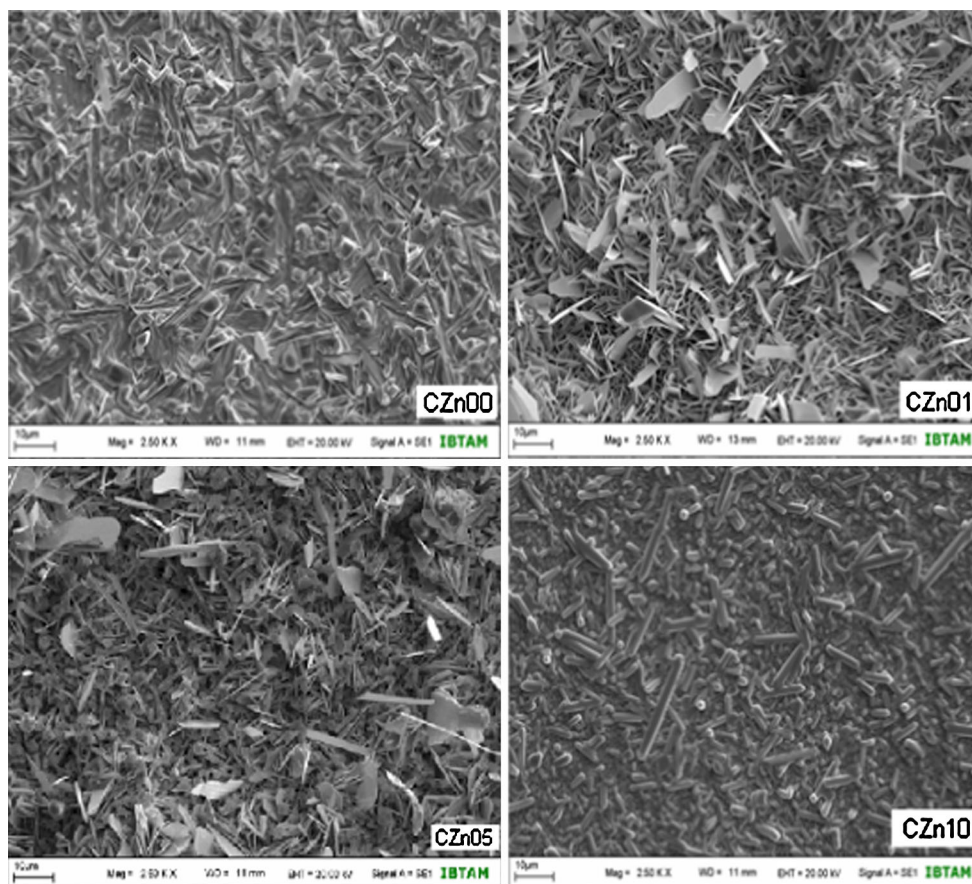


Fig. 3 SEM micrographs of the samples

Table 2 Variation of element concentrations from EDS measurements for CZn00 and CZn10 samples

Elt.	Intensity (c/s)		Conc.	
	x = 0.0	x = 1.0	x = 0.0	x = 1.0
Ca	13.66	11.82	23.09	22.25
Cu	55.53	29.41	59.22	34.93
Zn	–	13.61	–	15.71
Sr	17.13	21.62	13.25	18.62
Bi	13.68	23.54	4.44	8.50
			100.00	100.00

Vickers microhardness test measurements were performed in this study, using the digital microhardness device at room temperature to determine the doping effect on the mechanical properties of the samples. The load, *F*, is applied for 10 s and changed in the range of 0.245–2.940 N. Indenter is suppressed on the different points of the samples. Vickers microhardness values are calculated using the diagonal length of the indentation (Eq. 1).

$$H_v = 1,854.4 \left(\frac{F}{d^2} \right) \text{ (GPa)} \tag{1}$$

Figure 5 shows the variation of Vickers microhardness results as a function of the applied load for all samples. As can be seen from this figure, microhardness value of undoped CZn00 sample increases with the applied load, which is known as RISE behavior in the literature. On the other hand, the microhardness of CZn01, CZn05 and CZn10 samples decreased with applied load. The decrease in the microhardness values, depending on doping rates and applied load are related with impurity phases and irregular grain orientation distribution. For these samples, the microhardness values are load dependent which shows ISE behavior. Behavior of the materials is changed with the Zn doping. The microhardness values of these samples are higher at lower applied loads, but they decrease as the applied load is increased. The microhardness values reaches to plateau limit at about 2 N for CZn00 sample. The hardness-load curve shows a transition to the plateau limit for higher values of applied load. The plateau values of microhardness correspond to the load independent (intrinsic) microhardness values [25]. As a result,

Fig. 4 Results of EDS measurements of CZn00 and CZn10 samples

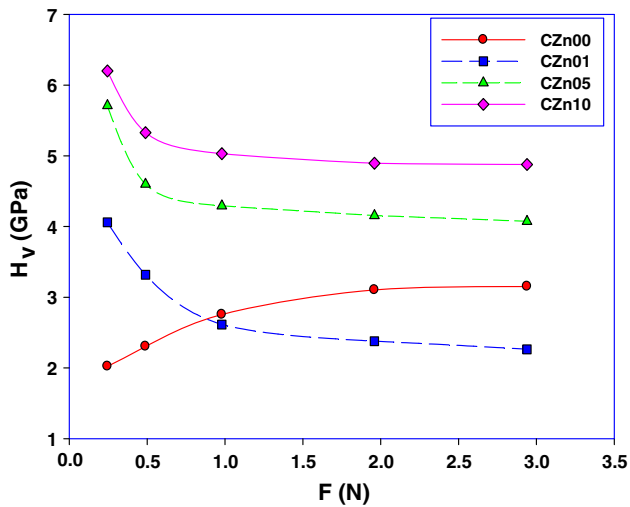
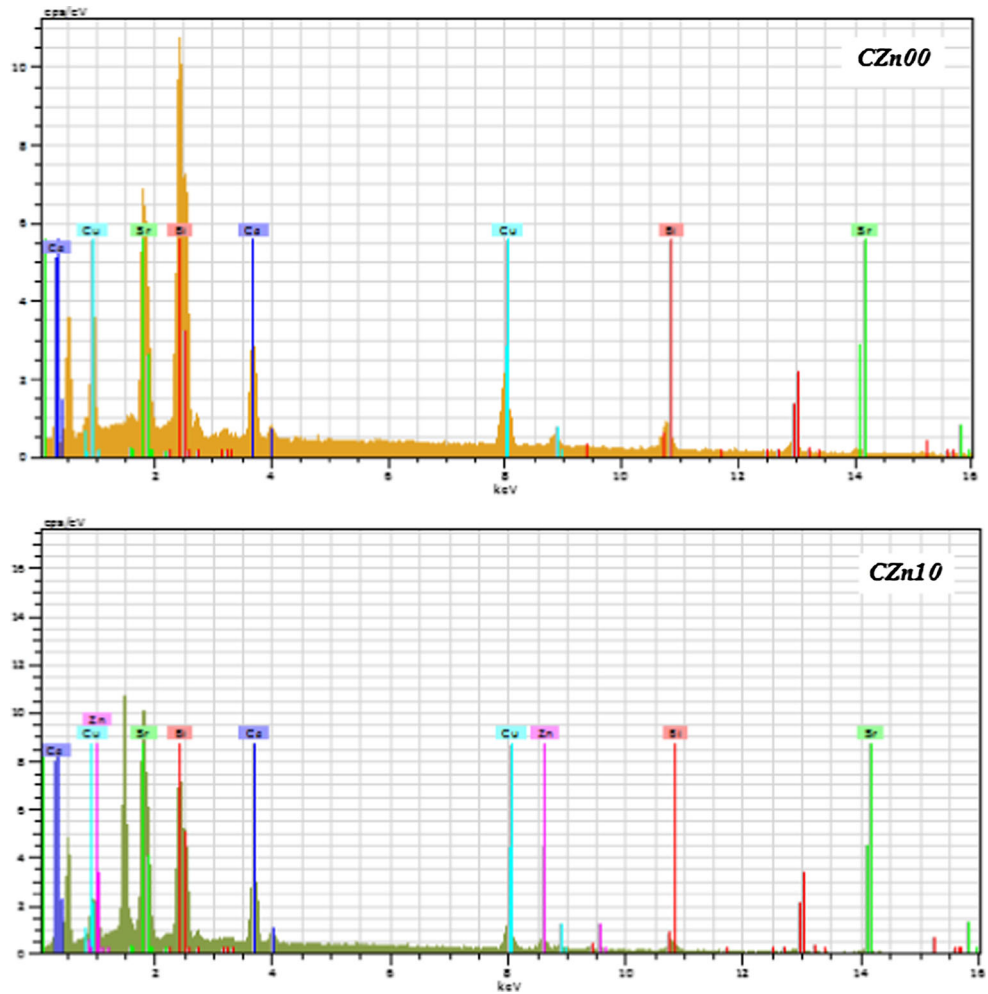


Fig. 5 Variations of microhardness with applied load for the samples

behavior of the material changed with increasing of Zn doping. Also, the hardness increased with increasing Zn doping.

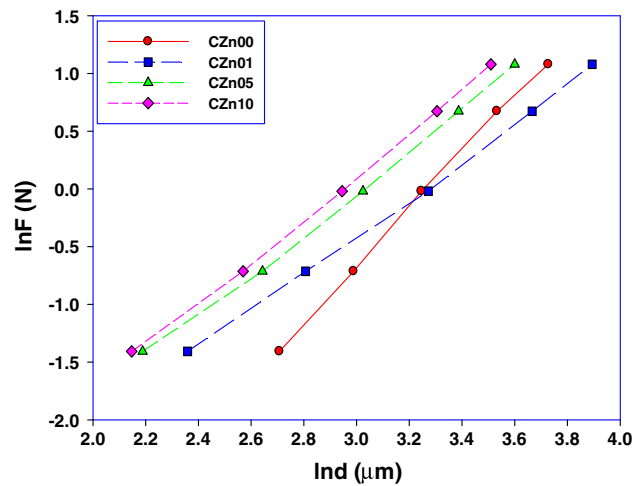


Fig. 6 Variation of applied load $\ln F$ with diagonal lnd for the samples

The calculated results of load dependent H_v , elastic modulus (E), yield strength (Y), and fracture toughness (K_{IC}) values calculated by Eqs. (1–4) are given in Table 3.

Table 3 The calculated values of load dependent H_v , E , Y and K_{IC} for the samples

Samples	Load (N)	H_v (GPa)	E (GPa)	Y (GPa)	K_{IC} (Pa/m ^{1/2})
CZn00	0.245	2.022	165.725	0.674	2,281.17
	0.490	2.304	188.826	0.768	2,434.98
	0.980	2.756	225.871	0.919	2,663.14
	1.960	3.104	254.402	1.035	2,826.34
	2.940	3.153	258.465	1.051	2,848.83
CZn01	0.245	4.059	332.674	1.353	3,232.02
	0.490	3.317	271.909	1.106	2,921.98
	0.980	2.613	214.205	0.871	2,593.46
	1.960	2.377	194.862	0.792	2,473.59
	2.940	2.262	185.432	0.754	2,413.00
CZn05	0.245	5.710	468.016	1.903	3,833.5
	0.490	4.597	376.747	1.532	3,439.45
	0.980	4.291	351.689	15.707	3,323.11
	1.960	4.154	340.474	1.385	3,269.69
	2.940	4.072	333.769	1.357	3,237.34
CZn10	0.245	6.200	508.209	2.067	3,994.72
	0.490	5.327	436.650	1.776	3,702.81
	0.980	5.029	412.179	1.676	3,597.56
	1.960	4.895	401.187	1.632	3,549.26
	2.940	4.878	399.851	1.626	3,543.35

Table 4 Best-fit results of experimental data according to Meyer’s law

Samples	n_K	$\ln A_{1K}$ (GPa)	H_v (GPa)
CZn00	2.46	−8.06	3.104–3.153
CZn01	1.61	−5.23	2.262–2.613
CZn05	1.77	−5.34	4.072–4.291
CZn10	1.83	−5.37	4.878–5.029

$$E = 81.9635H_v \tag{2}$$

$$Y \approx H_v/3 \tag{3}$$

$$K_{IC} = \sqrt{2E\gamma} \tag{4}$$

As microhardness changes with applied load, real value of microhardness is indefinite. Some models are developed to explain ISE and RISE behavior in the literature. In this study, Meyer’s law, HK approach, proportional sample resistance model, modified proportional sample resistance model, elastic/plastic deformation model and induced indentation cracking model are used to analyze microhardness results of our samples.

3.4.1 Analysis according to Meyer’s law

Meyer’s law is a frequently used model to explain ISE and RISE behavior. This law is a simple expression between applied load F and diagonal length d ,

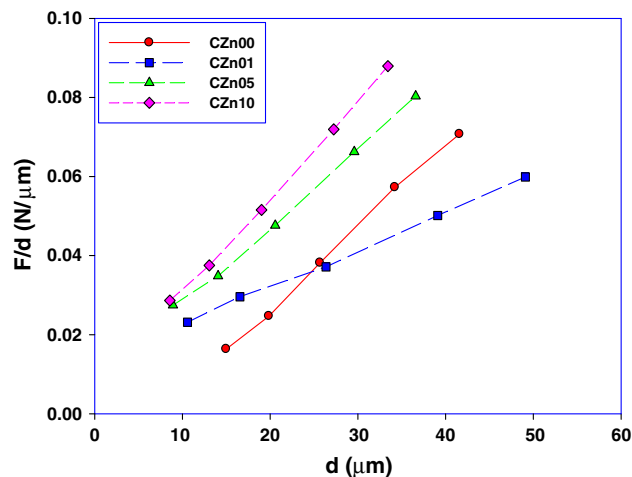


Fig. 7 Plots of F/d versus d for the samples

Table 5 Best-fit results of experimental data according to PSR model

Samples	$\alpha \times 10^{-2}$ (N/mm)	$\beta \times 10^{-3}$ (N/mm)	H_{PSR} (GPa)	H_v (GPa)
CZn00	157	2.1	3.894	3.104–3.153
CZn01	132	0.9	1.669	2.262–2.613
CZn05	86	1.9	3.523	4.072–4.291
CZn10	68	2.4	4.451	4.878–5.029

Table 6 The calculated values of load independent H_v , E , Y and K_{IC} for the samples

Samples	E_o (GPa)	Y_o (GPa)	K_{IC} (Pa/m ^{1/2})	H_v (GPa)
CZn00	319.17	1.30	3,165.72	3.104–3.153
CZn01	136.80	0.56	1,900.38	2.262–2.613
CZn05	288.76	1.17	2,228.59	4.072–4.291
CZn10	364.82	1.48	2,227.45	4.878–5.029

$$F = Ad^{n_K} \tag{5}$$

Here, n_K is Meyer exponent and is obtained from the curves that are fit with the experimental data (Fig. 6). n_K is also evaluated as the measure of ISE and RISE behaviors. If the n_K value is greater than 2, RISE behavior is obtained, If the n_K value is less than 2, ISE behavior is obtained. When n_K value is equal to 2, hardness is load independent, which gives the Kick’s law [14, 26–28].

The slope of the graph in Fig. 6 gives n_K , and the vertical intercept is A_{1K} . For undoped CZn00 sample, Meyer number is greater than 2, which proves the load dependent displacement has RISE behavior. For other Zn doped samples, Meyer number is less than 2, which proves the load dependent displacement has ISE behavior. The results obtained from the graph are given in Table 4.

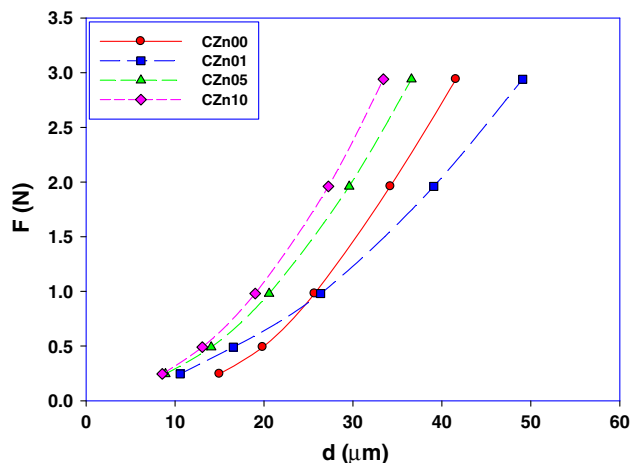


Fig. 8 Plots of F versus d for the samples

Table 7 Best-fit results of experimental data according to MPSR model

Samples	A_{0MPSR}	A_{1MPSR}	W_{MPSR} (N)	H_{MPSR} (GPa)	H_v (GPa)
CZn00	0.0073	0.0019	0.1029	3.523	3.104–3.153
CZn01	0.0095	0.001	0.0391	1.854	2.262–2.613
CZn05	0.001	0.0021	0.0627	3.894	4.072–4.291
CZn10	0.0031	0.0027	0.0776	5.006	4.878–5.029

3.4.2 Analysis according to PSR model

Another model to analyze the ISE behavior is proportional sample resistance (PSR) model. Li and Bradt [29] reported that PSR model is suitable to explain ISE behavior in various materials. The following expression is used in this model:

$$F = \alpha d + \beta d^2 \quad (6)$$

where, α is the surface energy and β is a parameter in order to calculate the real hardness value. α and β are calculated from Fig. 7. The change in the value of α is related to the energy dispersion of surface cracks [30]. Load-independent hardness value in PSR model is calculated from

$$H_{PSR} = 1,854.4\beta \quad (7)$$

In Table 5, values of α , β and H_{PSR} are given. Here, α is positive for all samples confirming that there is also elastic deformation as well as plastic deformation in all samples showing ISE behavior. When we compare the microhardness values of the samples calculated using PSR model [25, 31, 32], that are given in Table 4, they are far from the values of the plateau region obtained from Fig. 7.

In addition, load independent elastic modulus (E), yield strength (Y) and fracture toughness (K_{IC}) values are

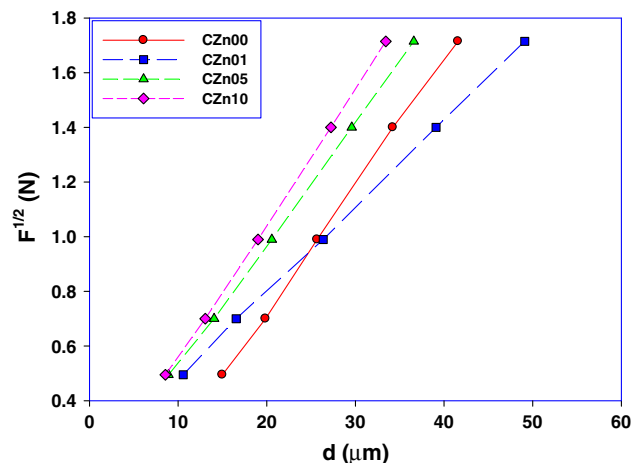


Fig. 9 Plots of square root of applied loads versus diagonal length for the samples

Table 8 Best-fit results of experimental data according to EPD model

Samples	A_2 (N/mm ²)	d_c (mm)	H_{EPD} (GPa)	H_v (GPa)
CZn00	0.046	-0.20	3.923	3.104–3.153
CZn01	0.031	0.16	1.782	2.262–2.613
CZn05	0.044	0.08	3.590	4.072–4.291
CZn10	0.049	0.06	4.452	4.878–5.029

calculated by Eqs. (2–4) using the load independent H_{PSR} values and these values were given in Table 6.

When compared with the load dependent values, load independent E_o , Y_o and K_{IC} values increased for undoped samples, but decreased for Zn doped CZn01, CZn05 and CZn10 samples. The decrease in the value of K_{IC} is related with the reduction of surface energy α . Fracture toughness (K_{IC}), is one of the important mechanical property of ceramic samples. The selection of materials used for technological applications is an important parameter. Elastic and plastic deformations are observed on the materials obeying ISE behavior. So, a relaxation occurs on the sample surface after the indenter removed. This situation causes a decrease in the hardness of the material. If the materials have RISE behavior, only elastic deformation is observed. Toughness also decreases or increases due to the fact that the hardness of the samples decreased or increased. We can say that the obtained results are also consistent with the literature [33, 34].

3.4.3 Analysis according to modified PSR (MPSR) model

According to this model, the physical meaning of A_{0MPSR} and A_{1MPSR} parameters are the same as the ones in PSR

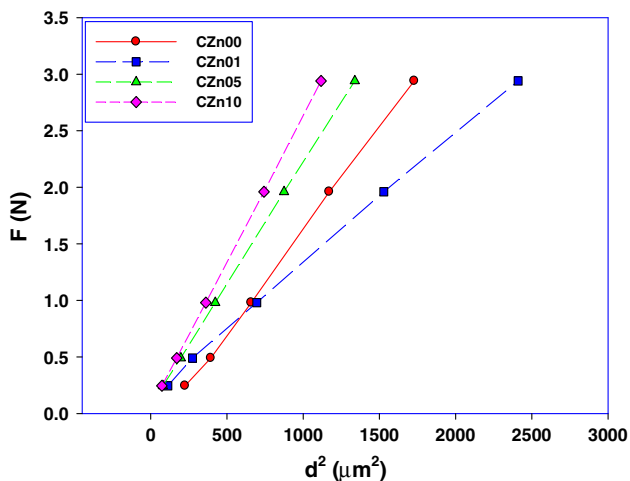


Fig. 10 Applied load versus the square of the impression semi-diagonal length for the samples

Table 9 Best-fit results of experimental data according to HK model

Samples	C_1	W_{HK} (N)	H_{HK} (GPa)	H_v (GPa)
CZn00	0.0018	-0.19	3.337	3.104–3.153
CZn01	0.0012	0.15	2.225	2.262–2.613
CZn05	0.0021	0.07	3.894	4.072–4.291
CZn10	0.0026	0.05	4.821	4.878–5.029

model [25]. MPSR model is defined with the following equation;

$$F = W_{MPSR} + A_{0MPSR}d + A_{1MPSR}d^2 \tag{8}$$

The load independent microhardness value due to MPSR model can be calculated using;

$$H_{MPSR} = 1,854.4 A_{1MPSR} \tag{9}$$

W_{MPSR} and A_{MPSR} values obtained by fit of Fig. 8 and load-independent hardness values related with these parameters are given in Table 7. As can be seen from this table, load-independent hardness values, calculated according to the MPSR model, are so far from results in the plateau region.

3.4.4 Analysis according to elastic/plastic deformation (EPD) model

According to Bull et al. [15, 35], the dependence of indentation size on the applied load is given as;

$$F = A_2(d_p + d_e)^2 \tag{10}$$

where, A_2 gives the load independent hardness constant. Here, d_e (elastic deformation) is related to the d_p (plastic deformation). The values of d_e and A_2 are calculated by the

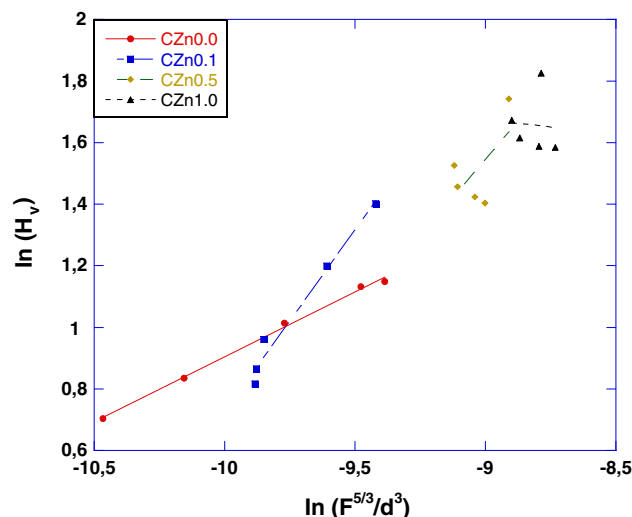


Fig. 11 Plots of $\ln H_v$ versus $\ln(F^{5/3}/d^3)$ for the samples

variation of the square root of applied load ($F^{1/2}$) with the indentation size (d) as depicted in Fig. 9. Besides, the load independent microhardness value due to this model is computed by following relation,

$$H_{EPD} = 1,854.4 A_2 \tag{11}$$

All the values obtained according to EPD model are listed in Table 8. It is seen from this table, the value of d_e is found to be negative for the undoped CZn00 sample, which means that there is not any clue on the elastic deformation in the material. The elastic recovery is observed for CZn00 sample exhibiting the RISE behavior, confirming that both the elastic and plastic deformations are produced in all samples except CZn00 under the applied load. However, the value of d_e is positive for doped samples. That means for this range of applied loads elastic deformation is observed along with plastic deformation. For these samples elastic relaxation is present. Presence of elastic deformation along with plastic deformation is the reason of ISE behavior for our samples.

As a result, as can be seen from Table 8, load-independent hardness values, calculated according to the EDP model, are so far from results in the plateau region.

3.4.5 Analysis according to Hays–Kendall approach

The microhardness measurements data on dependence of H_v on applied indentation test load can be explained by the HK approach [36]. Hays and Kendall suggested that, there exists a minimum applied test load W , necessary to initiate plastic deformation, which only elastic deformation occurs (Fig. 10).

$$F_{eff} = F_{max} - W = C_1d^2 \tag{12}$$

Table 10 Best-fit results of experimental data according to IIC model

Samples	m	$K \times 10^4 [N^{(3-5m)/3} / \mu m^{(2-3m)}]$	H_{IIC} (GPa)	H_V (plateau region) (GPa)
CZn00	0.42	0.016	2.590	3.104–3.153
CZn01	1.17	26.83	3.133	2.262–2.613
CZn05	0.98	3.28	4.696	4.072–4.291
CZn10	0.84	0.91	5.542	4.878–5.029

Table 11 The results of load dependent Vickers microhardness at the plateau region and load independent hardness values calculated using PSR, MPSR, EPD, HK and IIC models

Samples	H_{PSR} (GPa)	H_{MPSR} (GPa)	H_{EPD} (GPa)	H_{HK} (GPa)	H_{IIC} (GPa)	H_V (GPa) (in plateau region)
CZn00	3.894	3.523	3.923	3.337	2.590	3.104–3.153
CZn01	1.669	1.854	1.782	2.225	3.133	2.262–2.613
CZn05	3.523	3.894	3.590	3.894	4.696	4.072–4.291
CZn10	4.451	5.006	4.452	4.821	5.542	4.878–5.029

Here, C_1 denotes a constant related to the applied test load and W shows the minimum load necessary to initiate the permanent deformation. The load independent W and C_1 values are summarized in Table 9.

As seen from Table 9, the value of W_{HK} is positive for the Zn-doped samples exhibiting the ISE behavior whereas the undoped sample showing the RISE behavior obtains the negative value of W_{HK} . It may be attributed to the fact that the positive value is sufficient to produce the elastic (reversible) deformation as well as the plastic (irreversible) deformation in the materials. On the other hand, the negative W_{HK} value is due to dominant characterization of the plastic deformation in the system [35]. According to this result, elastic deformation was observed on CZn01, CZn05 and CZn10 pellet samples.

The hardness value obtained with HK model is closer the hardness value in the plateau region. It is underlined that the load independent hardness value should have been close to value of the plateau region in the studies on different materials in the literature [25, 37, 38]. For this reason, HK model is the most appropriate model in the analysis of microhardness and determining the mechanical properties of CZn01, CZn05 and CZn10 samples showing the ISE behavior.

3.4.6 Analysis according to indentation-induced cracking (IIC) model

This model is developed by Li and Bradt [29] to explain the RISE behavior. Depending on the model, applied test load

is equilibrated by the total sample resistance in the maximum depth. According to Li and Bradt, friction (slip) and elastic affects lead to the normal ISE behavior. In this model, hardness value is obtained by the equation:

$$H_V = \lambda_1 K_1 \left(\frac{P}{d^2} \right) + K_2 \left(\frac{P^{5/3}}{d^3} \right) \quad (13)$$

where, d is the diameter of the indenter, λ_1 , K_1 and K_2 are constants. The constant K_1 value changes with the indenter geometry and K_2 depends on the applied load.

For a perfect plastic material $H_V = K_1(P/d^2)$, $\lambda_1 = 1$ and $K_2(P^{5/3}/d^3) = 0$, whereas for perfect brittle solids $H_V = K_2(P^{5/3}/d^3)$ and $\lambda_1 = 0$. If the examined material is a brittle material, only the second part of the equation is used, as described below. In this study, elastic deformation was not observed in Zn undoped sample. Hence, Eq. 13 can be rewritten as,

$$H_V = K \left(\frac{P^{5/3}}{d^3} \right)^m \quad (14)$$

where, K and m demonstrate load independent constants. The variation of microhardness value $\ln(H_V)$ with $\ln(P^{5/3}/d^3)$ for all the samples is given in Fig. 11. The extracted values of K , m and H_{IIC} are illustrated in Table 10. The value of m is used to describe the ISE behavior for $m > 0.6$ whereas $m < 0.6$ points out the RISE behavior [33, 39, 40].

In the hardness analysis, this model only the most appropriate for undoped material showing the RISE behavior. As it is seen from Table 10, the power value, m , is obtained to be about 1.17, 0.98 and 0.84 for the CZn01, CZn05 and CZn10 samples, respectively, whereas the value of m is found to be about 0.42 for CZn00 sample, meaning that the Zn-doped samples exhibit the ISE behavior while the undoped sample obeys the RISE behavior (Table 11).

4 Conclusion

In this study, the effects of Zn doping on structural and mechanical properties of $\text{Bi}_{1.8}\text{Sr}_2\text{Ca}_2\text{Cu}_{3.2-x}\text{Zn}_x\text{O}_{10+\delta}$ ($x = 0.0, 0.1, 0.5, 1.0$) samples have been investigated. Therefore, XRD, SEM, EDS and microhardness measurements were done. The XRD analysis showed that the lattice constant a increased with increasing the Zn doping while, b and c initially increased and then decreased with increasing the Zn doping. SEM results showed that crystallization of the sample increased with increasing the Zn doping. Sample crystallized partially and the amorphous matrix began to decline with doping. In addition, a significant decrease was observed in the percentage of Cu from EDS measurements. Compared to other elements, this

result is the indication of Zn atoms, in the doped structure, entered into crystal structure substituting the Cu atoms, predominantly. Microhardness measurements were performed to investigate the effect of Zn doping on the mechanical properties of materials. The increase in the microhardness values of the undoped CZn00 sample depends on the increase of applied load, which shows RISE behavior. The microhardness of CZn01, CZn05 and CZn10 samples decreased with applied load. For these samples, the microhardness values are load dependent which shows ISE behavior. Behavior of the materials is changed with Zn doping. In order to investigate this behavior, some models have been used (Meyer Law, the PSR model, MPSR Model, EPD Model, IIC Model and HK approach). When all models were applied on the samples, it has been concluded that HK approach is the most suitable model for CZn00 sample showing ISE behavior and IIC model is the most suitable model for CZn01, CZn05 and CZn10 samples showing RISE behavior.

Acknowledgments The authors thank the financial support for this work through the Scientific Research Projects (BAP 05/2011-47) Foundation of Gazi University Ankara.

References

1. H. Maeda, Y. Tanaka, M. Fukutomi, T. Asano, A new high Tc oxide superconductor without a rare earth element. *Jpn. J. Appl. Phys.* **27**, 209–210 (1988)
2. M. Nursoy, M. Yilmazlar, C. Terzioglu, I. Belenli, Transport, microstructure and mechanical properties of Au diffusion-doped Bi-2223 superconductors. *J. Alloy Compd.* **459**, 399–406 (2008)
3. M.U. Herrera, R.V. Sarmago, Synthesis of Pb-doped Bi-2223 from Pb-doped Bi-2212 via partial melting. *Ceram. Int.* **30**, 1611–1614 (2004)
4. H. Zhang, K. Wu, Q.R. Feng, X. Zhu, F.X. Chen, S.Q. Feng, X.Y. Zhou, Carrier character of Bi containing 2223 phase doped by Mo and W. *Phys. Lett. A* **169**, 214–218 (1992)
5. N. Miura, F. Sakata, Y. Shimizu, Y. Deshimaru, N. Yamazoe, Tc enhancement of excess Sr-doped Bi-2223 oxides by control of oxygen content. *Phys. C* **235**, 479–480 (1994)
6. H. Koralay, A. Arslan, S. Cavdar, O. Ozturk, E. Asikuzun, A. Gunen, A.T. Tasci, Structural and mechanical characterization of Bi_{1.75}Pb_{0.25}Sr₂Ca₂Cu_{3-x}Sn_xO_{10+y} superconductor ceramics using Vickers microhardness test. *J. Mater. Sci. Mater. Electron.* **24**, 4270–4278 (2013)
7. U. Kolemen, O. Uzun, M. Yilmazlar, N. Guclu, E. Yanmaz, Hardness and microstructural analysis of Bi_{1.6}Pb_{0.4}Sr₂Ca_{2-x}Sm_xCu₃O_y polycrystalline superconductors. *J. Alloys Compd.* **415**, 300–306 (2006)
8. S. Cavdar, E. Deniz, H. Koralay, O. Ozturk, M. Erdem, A. Gunen, The effect of PbSe addition on the mechanical properties of Bi-2212 superconductors. *J. Supercond. Nov. Magn.* **25**, 2297–2307 (2012)
9. J. Sun, L.F. Francis, W.W. Gerberich, Mechanical properties of polymer-ceramic nanocomposite coatings by depth-sensing indentation. *Polymer Eng. Sci.* **45**, 207–216 (2005)
10. G.R. Sawyer, P.M. Sargent, T.F. Page, Microhardness anisotropy of silicon carbide. *J. Mater. Sci.* **15**(4), 1001–1013 (1980)
11. O. Ozturk, M. Erdem, E. Asikuzun, O. Yildiz, G. Yildirim, A. Varilci, C. Terzioglu, Investigation of indentation size effect (ISE) and micro-mechanical properties of Lu added Bi₂Sr₂CaCu₂O_y ceramic superconductors. *J. Mater. Sci. Mater. Electron.* **24**, 230–238 (2013)
12. Q. Ma, D.R. Clarke, Size dependent hardness of silver single crystals. *J. Mater. Res.* **10**, 853–864 (1995)
13. O. Uzun, T. Karaaslan, M. Gogebakan, M. Keskin, Hardness and microstructural characteristics of rapidly solidified Al–8–16 wt% Si alloys. *J. Alloys Compd.* **376**, 149–157 (2004)
14. E. Asikuzun, O. Ozturk, H.A. Cetinkara, G. Yildirim, A. Varilci, M. Yilmazlar, C. Terzioglu, Vickers hardness measurements and some physical properties of Pr₂O₃ doped Bi-2212 superconductors. *J. Mater. Sci. Mater. Electron.* **23**, 1001–1010 (2012)
15. S.J. Bull, T.F. Page, E.H. Yoffe, An explanation of the indentation size effect in ceramics. *Philos. Mag. Lett.* **59**, 281–288 (1989)
16. J. Gong, On the energy balance model for conventional Vickers microhardness testing of brittle ceramics. *J. Mater. Sci. Lett.* **19**, 515–517 (2000)
17. H. Huang, P. Hing, Energy balance model for the Vickers hardness of ferroelectric PZT ceramics. *J. Mater. Sci. Lett.* **18**, 1675–1677 (1999)
18. J. Gong, Y. Li, An energy-balance analysis for the size effect in low-load hardness testing. *J. Mater. Sci.* **35**, 209–213 (2000)
19. J. Guille, M. Sieskind, Microindentation studies on BaFCl single crystals. *J. Mater. Sci.* **26**, 899–903 (1991)
20. R.E. Hanneman, J.W. Westbrook, Effects of adsorption on the indentation deformation of non-metallic solids. *Philos. Mag.* **18**, 73–88 (1968)
21. T. Kavetskiy, J. Borc, K. Sangwal, V. Tsmots, J. Filipecki, M. Iovu, Vickers microhardness testing of indentation size effect in some metal-modified chalcogenide glasses. *Adv. Nat. Sci. Theory Appl.* **1**, 183–196 (2012)
22. K. Sangwal, Microhardness of as-grown and annealed lead sulphide crystals. *J. Mater. Sci.* **24**, 1128 (1989)
23. A. Biju, U. Syamaprasad, R. Ashok, J.G. Xu, K.M. Sivakumar, Y.K. Kuo, Structural and transport properties of Nd doped (Bi,Pb)-2212. *Phys. C* **46**, 69–75 (2007)
24. O. Ozturk, E. Asikuzun, M. Coskunyurek, N. Soyulu, A. Hancerliogullari, A. Varilci, C. Terzioglu, The effect of Nd₂O₃ addition on superconducting and structural properties and activation energy calculation of Bi-2212 superconducting system. *J. Mater. Sci. Mater. Electron.* **25**, 444–453 (2013)
25. J.B. Quinn, V.D. Quinn, Indentation brittleness of ceramics: a fresh approach. *J. Mater. Sci.* **32**, 4331–4346 (1997)
26. O. Ozturk, H.A. Cetinkara, E. Asikuzun, M. Akdogan, M. Yilmazlar, C. Terzioglu, Investigation of mechanical and superconducting properties of iron diffusion-doped Bi-2223 superconductors. *J. Mater. Sci. Mater. Electron.* **22**, 1501–1508 (2011)
27. O. Ozturk, E. Asikuzun, G. Yildirim, The role of Lu doping on microstructural and superconducting properties of Bi₂Sr₂CaLu_xCu₂O_y superconducting system. *J. Mater. Sci. Mater. Electron.* **24**, 1274–1281 (2013)
28. L. Arda, O. Ozturk, E. Asikuzun, S. Ataoglu, Structural and mechanical properties of transition metals doped ZnMgO nanoparticles. *Powder Technol.* **235**, 479–484 (2013)
29. H. Li, R.C. Bradt, The microhardness indentation load/size effect in rutile and cassiterite single crystals. *J. Mater. Sci.* **28**, 917–926 (1993)
30. H.A. Cetinkara, M. Yilmazlar, O. Ozturk, M. Nursoy, C. Terzioglu, The influence of cooling rates on microstructure and mechanical properties of Bi_{1.6}Pb_{0.4}Sr₂Ca₂Cu₃O_y superconductors. *J. Phys. Conf. Ser.* **153**, 012038 (2009)

31. M. Yilmazlar, O. Ozturk, O. Gorur, I. Belenli, C. Terzioglu, Role of diffusion-annealing time on the mechanical properties of bulk Bi-2223 superconductors diffusion-doped with Au. *Supercond. Sci. Technol.* **20**, 365–371 (2007)
32. M. Yilmazlar, H.A. Cetinkara, M. Nursoy, O. Ozturk, C. Terzioglu, Thermal expansion and Vickers hardness measurements on $\text{Bi}_{1.6}\text{Pb}_{0.4}\text{Sr}_2\text{Ca}_{2-x}\text{Sm}_x\text{Cu}_3\text{O}_y$ superconductors. *Phys. C* **442**, 101–107 (2006)
33. K. Sangwal, On the reverse indentation size effect and microhardness measurement of solids. *Mater. Chem. Phys.* **63**, 145–152 (2000)
34. M.B. Turkoz, S. Nezir, O. Ozturk, E. Asikuzun, G. Yildirim, C. Terzioglu, A. Varilci, Experimental and theoretical approaches on mechanical evaluation of Y123 system by Lu addition. *J. Mater. Sci. Mater. Electron.* **24**, 2414–2421 (2013)
35. K. Inabe, K. Emoto, K. Sakamaki, R.N. Takeuchi, Length and microhardness of alkali halide crystals. *Jpn. J. Appl. Phys.* **11**, 1743–1753 (1972)
36. C. Hays, E.G. Kendall, An analysis of Knoop microhardness. *Metallography* **6**, 275–282 (1973)
37. J. Gong, Z. Zhao, Z. Guan, H. Miao, Load-dependence of Knoop hardness of $\text{Al}_2\text{O}_3\text{-TiC}$ composites. *J. Eur. Ceram. Soc.* **20**, 1895–1900 (2000)
38. Z.J. Peng, J.H. Gong, H.Z. Miao, Load-dependent indentation behavior of $\beta\text{-SiAlON}$ and $\alpha\text{-silicon carbide}$. *J. Eur. Ceram. Soc.* **24**, 2193–2201 (2004)
39. R. Awad, A.I. Abou-Aly, M. Kamal, M. Anas, Mechanical properties of (Cu 0.5Ti 0.5)-1223 substituted by Pr. *J. Supercond. Nov. Magn.* **24**, 1947–1956 (2011)
40. M. Tosun, S. Ataoglu, L. Arda, O. Ozturk, E. Asikuzun, D. Akcan, O. Cakiroglu, Structural and mechanical properties of ZnMgO nanoparticles. *Mater. Sci. Eng. A* **590**, 416–422 (2014)